Applied Catalysis B: Environmental 164 (2015) 288–296

Contents lists available at ScienceDirect

Applied Catalysis B: Environmental

journal homepage: www.elsevier.com/locate/apcatb

Search for reactive intermediates in catalytic oxidation with hydrogen peroxide over amorphous niobium(V) and tantalum(V) oxides

Maria Ziolek[a,*], Izabela Sobczak[a], Piotr Decyk[a], Kamila Sobańska[b], Piotr Pietrzyk[b,*], Zbigniew Sojka[b]

[a] Adam Mickiewicz University in Poznan, Faculty of Chemistry, ul. Umultowska 89b, 61-614 Poznan, Poland
[b] Jagiellonian Uniwersity, Faculty of Chemistry, ul. Ingardena 3, 30-060 Krakow, Poland

ARTICLE INFO

Article history:
Received 9 July 2014
Received in revised form 6 September 2014
Accepted 12 September 2014
Available online 22 September 2014

Keywords:
Superoxo and peroxo species
Hydroxyl radicals
Oxidation of glycerol and cyclohexene
H_2O_2 as oxidant
Nb_2O_5, Ta_2O_5

ABSTRACT

The reactive oxygen intermediates generated on surface of amorphous Nb_2O_5 and Ta_2O_5 upon interaction with aqueous H_2O_2 were identified. The role of dehydroxylation of the surface, pH of H_2O_2 solution, and the presence or absence of oxygen in gas phase were studied in depth by UV–Vis, FTIR, Raman, and EPR techniques. The study revealed high ability of the amorphous Nb_2O_5 to form peroxo, superoxo, and radical hydroxyl species upon contact with hydrogen peroxide. This process depends on the level of surface hydroxylation which is lower for amorphous Ta_2O_5 than amorphous Nb_2O_5. The relationship between the formation of superoxo and peroxo species and pH of the H_2O_2/H_2O solution was proved. Superoxo species interact with the excess of H_2O_2 towards hydroxyl radicals, which are the most active species in catalytic oxidation. The role of pH was evident in the oxidation of glycerol. NaOH and link of superoxo species to niobium enhance the reaction rate by increase of hydroxyl radicals number. The hydroxyl radicals are also the active species in the formation of hydroxylated cyclohexene and finally cyclohexenediol in cyclohexene oxidation.

1. Introduction

Hydrogen peroxide is often used as a powerful, environmentally friendly and safe oxidant ($2H_2O_2 \rightarrow 2H_2O + O_2$). For these reasons, it is also often used for removal of pollutants. To cope with more difficult-to-oxidize chemicals, hydrogen peroxide has to be activated with such catalysts as iron, copper, manganese, or other transition-metal based systems.

Depending on the properties of the catalyst surface, various types of O-O bond cleavage in H_2O_2 can occur (homolytic or heterolytic), and various types of oxidative species can be generated (hydroxyl and superoxide radicals, peroxide anions). The homolytic pathway proceeds via free radical mechanism. In the first step metal active species participate in a uniform cleavage of the O—O bond forming •OH radicals, which are the intermediates in subsequent oxidation processes. The heterolytic pathway takes place via oxometal or peroxometal species as active sites. In many cases homolytic and heterolytic pathways can afford the same products [1,2].

Many metals exhibit distinct electron transfer properties, which enhance their performance in activation of hydrogen peroxide (H_2O_2). By far, the most common of these is iron, which during the interaction with hydrogen peroxide gives rise to generation of highly reactive hydroxyl radicals (•OH). The reactivity of such system, called Fenton reagent, stems from an easy change in the oxidation state of iron cations upon interaction with H_2O_2, according to the scheme:

$$Fe^{2+} + H_2O_2 \rightarrow Fe^{3+} + OH^- + {}^{\bullet}OH \quad (1)$$

$$Fe^{3+} + H_2O_2 \rightarrow Fe^{2+} + {}^{\bullet}OOH + H^+ \quad (2)$$

The rates of catalytic reactions driven by Fenton reagent are generally limited by the rate of hydroxyl radicals formation. In aqueous media, the chemical reactions of hydroxyl radicals can be classified into the following categories:

Addition in which a hydroxyl radical is inserted to an unsaturated compound, aliphatic or aromatic, to form a free radical product (e.g. $^{\bullet}OH + C_6H_6 \rightarrow (OH)C_6H_6^{\bullet}$).

Hydrogen Abstraction where an organic free radical and water are formed (e.g. $^{\bullet}OH + CH_3OH \rightarrow {}^{\bullet}CH_2OH + H_2O$).

Radical Interaction in which a hydroxyl radical reacts with another hydroxyl (or different) radical, to recombine or to disproportionate to form a stable product (e.g. $^{\bullet}OH + {}^{\bullet}OH \rightarrow H_2O_2$).

* Corresponding author. Tel.: +48 605475381. (M. Ziolek), +48 12 6632224 (P. Pietrzyk)
E-mail addresses: ziolek@amu.edu.pl (M. Ziolek), pietrzyk@chemia.uj.edu.pl (P. Pietrzyk).

http://dx.doi.org/10.1016/j.apcatb.2014.09.024
0926-3373/

Hydroxyl radicals can be generated by direct interaction of metal-hydroxyl species with H_2O_2. Jorda, Tuel and co-workers [3] proposed the following scheme of such interaction between titanium oxide surface and hydrogen peroxide.

$$Ti–OH + H_2O_2 \rightarrow Ti–OOH + H_2O \quad (3)$$

$$Ti–OOH \rightarrow Ti–O^{\bullet} + {}^{\bullet}OH \quad (4)$$

$$Ti–O^{\bullet} + H_2O \rightarrow Ti–OH + {}^{\bullet}OH \quad (5)$$

The generated hydroxyl radicals were found to be active in cyclohexene oxidation to epoxide and cyclohexenyl hydroperoxide.

Although hydroxyl radicals belong to the most reactive chemical species, metal peroxo and metal oxo species were often postulated as active intermediates in the oxidation of organic compounds with H_2O_2 [1,2,4].

Hydrogen peroxide can react with a broad variety of inorganic and organic substrates in liquid-phase under very mild conditions. Specific interaction of H_2O_2 with the catalyst surface determines the nature of the resultant reactive oxygen species, their further transformation, and subsequent reaction with the oxidized molecules. Depending on the nature of the catalyst surface, various types of reactive oxygen species (OH^-, $OH^{\bullet}$, O_2^-, O_2^{2-}) can be generated upon the contact with H_2O_2. The focus in our previous study [5] was on H_2O_2 treatment of amorphous and crystalline niobium(V) and tantalum(V) oxides in the context of oxidation of glycerol to glycolic acid.

This continuation paper describes a more detailed study on the interaction of H_2O_2 with amorphous Nb_2O_5 and Ta_2O_5 under various conditions, and its impact on catalytic oxidation. The role of surface dehydroxylation, pH of the H_2O_2/H_2O solution, and the presence or absence of oxygen in a gas phase was studied by means of UV–Vis, FTIR, Raman, and EPR techniques. Oxidation of glycerol and cyclohexene were used as test reactions for the participation of various oxygen active species in the catalytic pathways of the oxidation process.

2. Experimental

2.1. Materials and H_2O_2 treatment

Amorphous Ta_2O_5 was prepared by precipitation of $Ta(C_2H_5O)_5$ in water, whereas commercial hydrated amorphous Nb_2O_5 was obtained from CBMM-Brazil. The samples of amorphous Nb_2O_5 and Ta_2O_5 were treated with 30% hydrogen peroxide (Merck) in order to generate active oxygen. This treatment was performed at room temperature by drop wise addition of hydrogen peroxide to metal oxides in the molar ratio H_2O_2/Nb(Ta) = 1:1.

2.2. UV–Vis spectroscopic study

The UV–Vis spectra were recorded on a Cary 300 Scan (Varian) spectrometer. The catalysts in the form of powder were placed in the cell equipped with a quartz window. The Kubelka-Munk (F(R)) plot was used to convert reflectance measurements into equivalent absorption spectra using the reflectance of SPECTRALON as a reference. The spectra were recorded in the range from 800 to 190 nm for both the parent amorphous metal oxides and the samples treated with 30% hydrogen peroxide. Two different atmospheres (oxygen or nitrogen) were used during the H_2O_2 treatment. UV-Vis spectra were also measured for Nb_2O_5 and Ta_2O_5 samples – dehydrated/dehydroxylated at increasing temperatures, and after H_2O_2 treatment of the dehydroxylated materials.

2.3. EPR study

Electron paramagnetic resonance (EPR) spectra were recorded with an X-band Bruker ELEXSYS-580 spectrometer, operating at 100 kHz field modulation using the 0.1–0.5 mT modulation amplitude. For the spectroscopic measurements typically 0.5 g of the catalyst was treated with 1.35 cm^3 of 30% H_2O_2. The pH was adjusted with 0.1 M NH_3 solution. After 3 days of the reaction the samples were dried in air at room temperature. Prior to the measurements the samples (0.01 g) were sealed in quartz tubes, and outgassed in a vacuum line ($p < 10^{-3}$ mbar) for 2 h at room temperature. The spectra were recorded at liquid nitrogen temperature (77 K). For liquid phase measurements, due to the limited stability of radicals formed during the reaction of H_2O_2 with the amorphous oxides, the spin trapping method was used. 5,5-Dimethyl-1-pyrroline N-oxide (DMPO), Sigma Aldrich, was chosen as a spin trap because of its well documented trapping ability and selectivity for oxygen-centered radicals. For qualitative experiments a small amount of the amorphous oxide was contacted with a mixture of 1 mL of 3% H_2O_2 and 10 μL of DMPO. The liquid was next transferred to a quartz capillary, and the EPR spectra were recorded at room temperature. The EPR parameters of the resultant spin adducts and the surface radicals were determined by simulation of the experimental spectra using the EPRsim32 package [6].

2.4. FTIR measurements

Prior to FTIR studies, the samples of amorphous Nb_2O_5 before and after reaction with H_2O_2 were pressed into self-supporting pellets. The spectra were recorded with a Bruker Tensor 27 spectrometer equipped with a MCT detector. The spectral resolution was equal to 2 cm^{-1}. Temperature-programmed reaction of H_2O_2 with amorphous niobia was carried out in situ at temperatures until 423 K, whereas the spectra were recorded at room temperature. Total concentration of the Brønsted acid sites was determined by quantitative IR studies using pyridine (Py) probe, as described elsewhere [7]. Prior to adsorption, the sample was activated in situ in an IR cell at 323 K ($p < 10^{-5}$ mbar) for 1 h. Sorption of pyridine was carried out at room temperature.

2.5. Raman spectroscopy

The microRaman analysis was performed with a Renishaw InVia dispersive spectrometer equipped with a CCD detector and integrated with a Leica DMLM confocal microscope. Two laser lines (785 nm and 514 nm) were checked to optimize the signal quality. The spectra were recorded at ambient conditions with the resolution of 2 cm^{-1}. The Raman scattered light was collected with a 50x Olympus objective in the spectral range of 100–1500 cm^{-1}. Nine scans were collected to assure a good signal-to-noise ratio.

2.6. Glycerol oxidation

Glycerol oxidation experiments were performed in a 300 cm^3 batch reactor (Parr). The oxidation reactions were carried out with hydrogen peroxide (0.2 or 0.6 M) at 333 K; 0.2 g of catalyst was added to a 1 M aqueous solution of glycerol followed by H_2O_2 admission (30%). The reaction was performed at pH = 5. By admission of NaOH (with NaOH/glycerol molar ratio of 2) pH was enhanced to 9.5, whereas by adding HNO_3 the pH was decreased to 2.5. Quantitative analysis of the reaction mixture was performed using a HPLC chromatograph (Waters) equipped with ultraviolet (UV) and refractive index (RI) detectors. The aliquots were taken at the end of the reaction, 1 cm^3 of the sample was diluted in 10 cm^3 of water and 5 μL of this solution was analyzed.

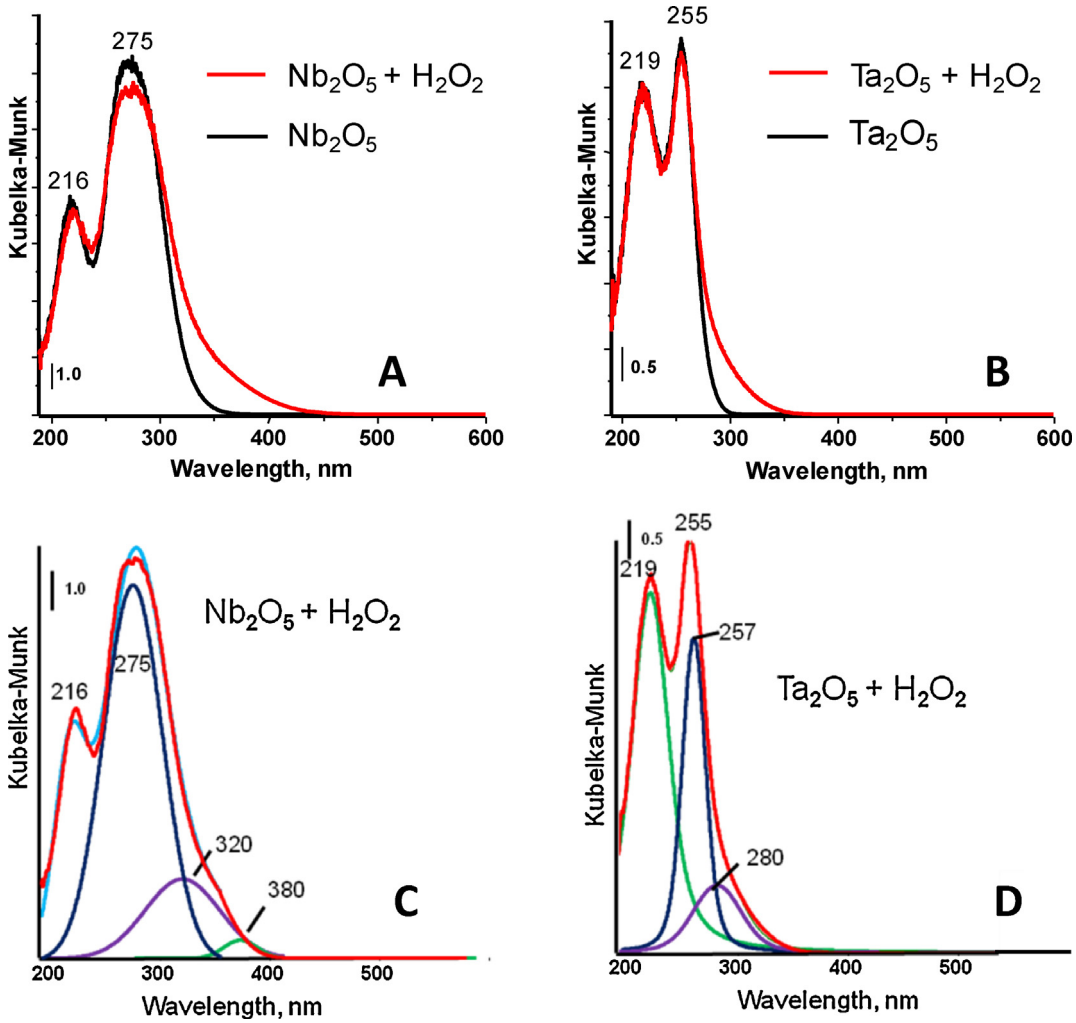

Fig. 1. UV–Vis spectra of Nb_2O_5 (A, C) and Ta_2O_5 (B, D) as purchased and treated with H_2O_2 (C, D–deconvoluted spectra).

2.7. Cyclohexene oxidation

The reaction was performed at 313 K in the liquid-phase using acetonitrile as a solvent. The catalytic reaction between cyclohexene and hydrogen peroxide was carried out in a glass flask equipped with a magnetic stirrer, a thermocouple, a reflux condenser, and a membrane for sampling. About 0.1 g of the catalyst outgassed at 473 K was placed in the flask, and next the solvent was added. The oxidation was conducted by efficient stirring of a mixture composed of 10 mL of acetonitrile (Fluka) and the catalyst at 313 K. After stirring for 15 min, 2 mmol of cyclohexene (Aldrich) was added, followed by one shot addition of 35% hydrogen peroxide (2 mmol). The pH of this mixture was ca 7. The samples were analysed at regular time intervals using a gas chromatograph Varian CP-3800 equipped with a capillary column DB-1 attached to a FID. For this purpose the heating program: 340 K for 15 min, ramp 10 K min^{-1} to 360 K (kept for 13 min) was used.

3. Results and discussion

3.1. The role of dehydroxylation of the surface and presence of oxygen

The study revealed high ability of amorphous Nb_2O_5 to form peroxo (O_2^{2-}) and superoxo (O_2^-) species upon the contact with hydrogen peroxide. The treatment of amorphous niobia samples with H_2O_2 led to significant change in colour from white to yellow, the latter being typical of the metal peroxo species [8]. This change was accompanied by distinct changes in the UV–Vis spectrum (Fig. 1A). The niobium(V) oxide treated with hydrogen peroxide showed an increase in the absorption intensity in the range 300–400 nm, assigned to charge transfer from O_2^- to niobium in niobium oxo species. Such assignment bases on the literature data [9] in which UV–Vis band at 344 nm for $NbO(O_2)_{0.5}PO_4{\cdot}2H_2O$ was related to charge-transfer processes (ligand-to-metal type) in the Nb-oxo-P system. The spectrum presented in Fig. 1A revealed that the absorption line increase in the region 300–400 nm after H_2O_2 treatment and it can be resolved into two bands at 320 and 380 nm, attributable to the ligand-to-metal charge transfer (LMCT) in a superoxo niobium and a peroxo niobium species, respectively (Fig. 1C). Assignment of the UV–Vis bands to the superoxo and peroxo species was based on the study of an aqueous H_2O_2/TS-1 system [10], where the bands at 360 and 405 nm, were associated with the LMCT in titanium superoxo and titanium peroxo species, respectively. The difference in the wavelengths in comparison with those presented for niobium superoxo and peroxo species is caused by the different energy level separation of the relevant orbitals.

Amorphous Ta_2O_5 interacted in a similar way with the hydrogen peroxide, but to a much lesser extent as it can be inferred from the UV–Vis spectrum (Fig. 1B), and did not change the colour of the sample. Deconvolution of the UV–Vis spectrum into component

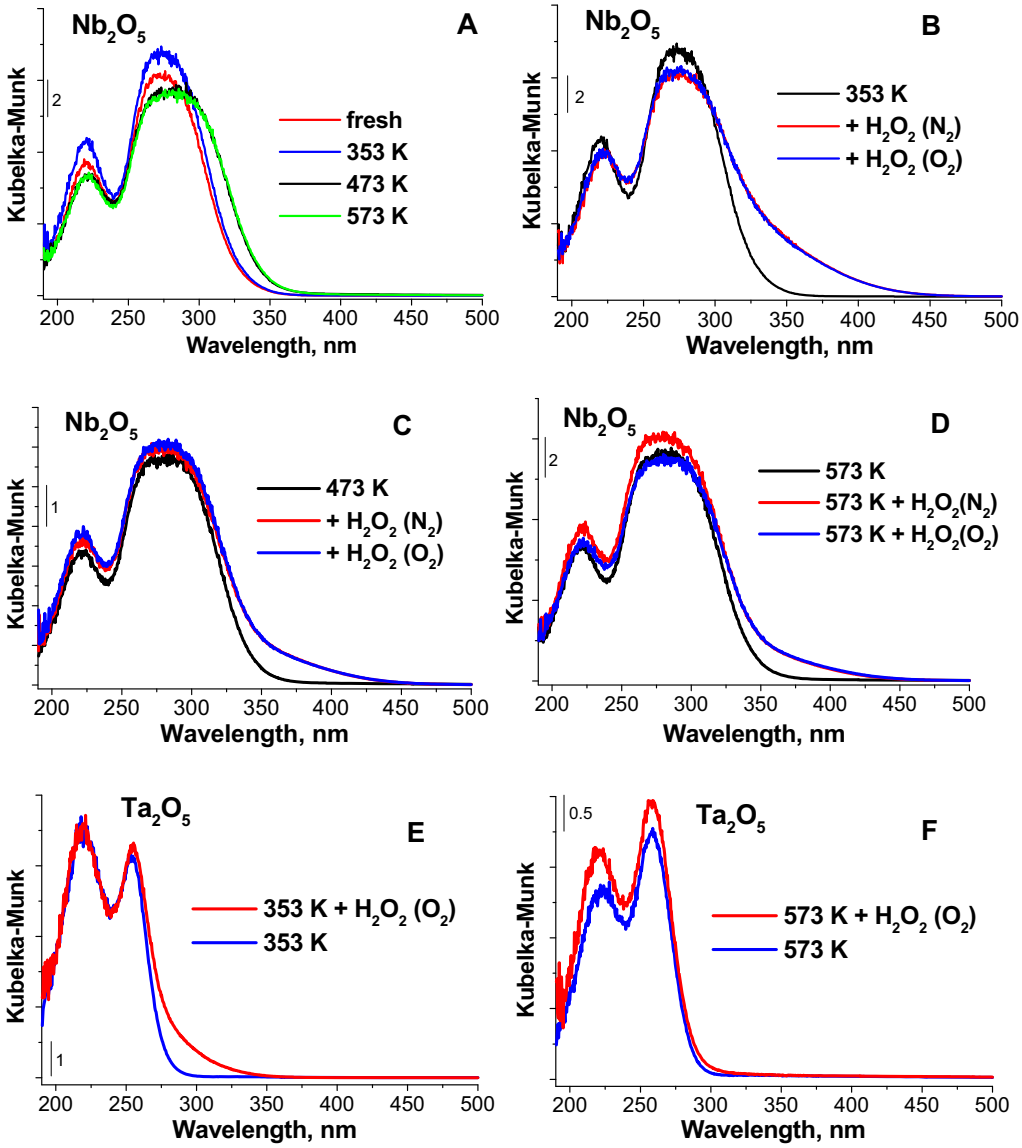

Fig. 2. UV–Vis spectra of Nb_2O_5 and Ta_2O_5: A- Nb_2O_5 outgased at different temperatures; B–D – Nb_2O_5 dehydroxylated at different temperatures and treated with H_2O_2 in oxygen or nitrogen atmosphere; E, F – Ta_2O_5 dehydroxylated at different temperatures and treated with H_2O_2 in oxygen atmosphere.

signals revealed formation of superoxo complex characterized by the LMCT band at 280 nm (Fig. 1D).

The shape of the UV–Vis spectra due to Nb_2O_5 depended markedly on the hydration level of the investigated oxide (Fig. 2A). Whereas dehydration of the sample at 353 K did not change the position and width of the UV–Vis bands, outgassing at 473 K shifted the maximum to higher wavelength and broadened the line. However, further increase in the temperature to 573 K did not change the shape and position of the spectrum. This effect was also observed in the case of Ta_2O_5, yet, because of its lower hydration level [5], it was less pronounced.

Insight into formation of the surface oxygen species after H_2O_2 treatment of the investigated oxides in the presence of gas-phase oxygen or nitrogen was obtained from UV–Vis measurements. As shown in Fig. 2B–D, the presence of nitrogen instead of oxygen did not change the shape, width and the intensity of the corresponding UV–Vis bands registered after outgassing at 353 K. Indeed, the UV–Vis spectra remained the same for Nb_2O_5 treated with hydrogen peroxide regardless the nature of the gas atmosphere. However, increase in the outgassing temperature from 353 to 473 and 573 K led to distinct reduction of the tail of the UV–Vis absorption. This tail covers the LMCT bands assigned to peroxo/hydroperoxo-niobium and superoxo-niobium moieties. Thus, one can postulate that increase in the dehydroxylation of Nb_2O_5 surface gives rise to decrease in surface concentration of those species. This effect was also observed for Ta_2O_5, but it was less marked due to the lower hydroxylation of Ta_2O_5 than that of Nb_2O_5 (Fig. 2E and F) [5].

3.2. The effect of Brønsted acidity

In order to determine what kind of surface hydroxyls participate in the interaction with H_2O_2, pyridine (Py) adsorption on amorphous Nb_2O_5 treated with hydrogen peroxide was studied. According to literature [11–13], when pyridine is coordinated to Lewis acid sites (LAS) the characteristic bands at ~ 1450 cm^{-1} and ~1610 cm^{-1} appear. The intensity of the first line is related to the number of LAS, whereas the position of the second band characterizes their strength. Adsorption of pyridine on Brønsted acid sites (BAS) gives a band at ~1550 cm^{-1} together with two other lines in the 1620–1640 cm^{-1} range, arising from vibrations of the pyridinium cations ($Py—H^+$). Moreover, pyridine can also interact

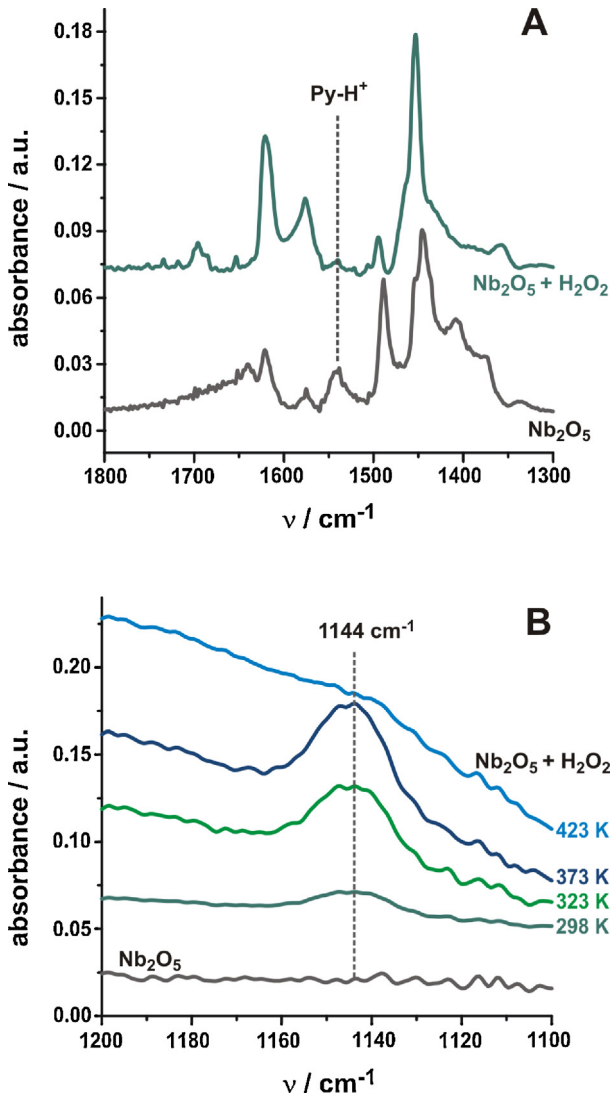

Fig. 3. In situ FTIR spectra of amorphous Nb_2O_5 (A) after pyridine adsorption at 298 K before and after reaction with H_2O_2 at RT, and (B) after reaction with H_2O_2 at RT followed by heating at increasing temperatures.

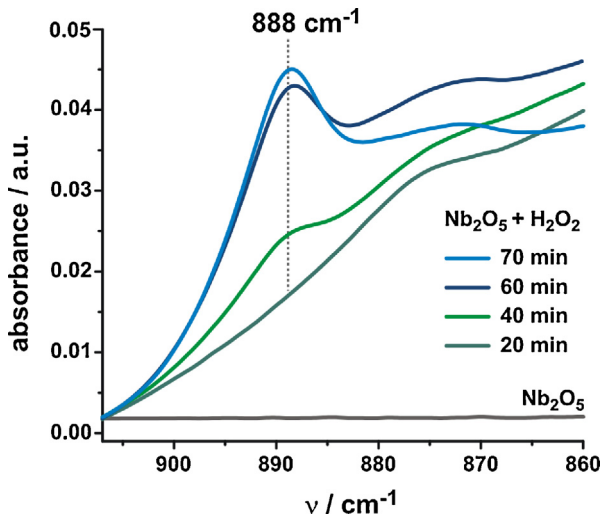

Fig. 4. ATR infrared spectra of amorphous Nb_2O_5 treated with H_2O_2 – formation of peroxo species depending on contact time.

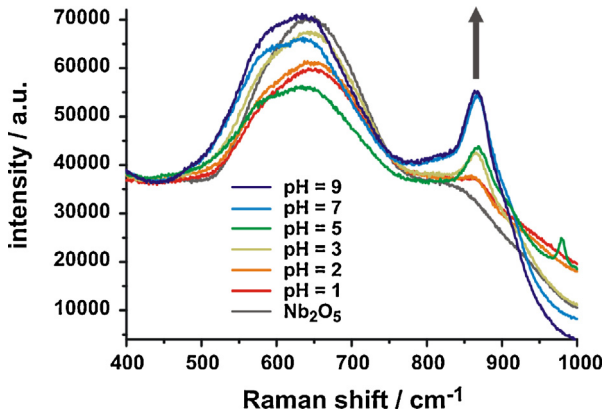

Fig. 5. Raman spectra of amorphous Nb_2O_5 treated with H_2O_2 at various pH.

with hydroxyls via hydrogen bonding, giving adsorption bands at 1596 cm^{-1} and 1445 cm^{-1}. The IR band at 1490 cm^{-1} is assigned to both, the pyridine coordinated to LAS and the pyridinium cations.

Niobium(V) oxide after pyridine adsorption exhibited IR bands assigned to pyridine attached to LAS, and the bands (the main at 1543 cm^{-1}) coming from Py—H^+ cations produced upon interaction with the surface BAS (Fig. 3A). It was found that the number of the acidic hydroxyls (BAS) substantially decreased from 100 μmol H^+/g to 24 μmol H^+/g after treatment of niobia with H_2O_2. It implies direct interaction of the acidic surface hydroxyls with hydrogen peroxide to form hydrosuperoxo species.

Consumption of acidic hydroxyls is accompanied by formation of surface reactive oxygen species probed with IR and Raman techniques. IR spectroscopy evidenced formation of the superoxo ($O_2^{-\bullet}$) entities owing to the presence of their characteristic band at 1144 cm^{-1} (Fig. 3B) due to O—O vibration [14,15]. Since superoxo groups are paramagnetic, their presence was additionally confirmed by EPR spectroscopy. A characteristic signal with partially resolved hyperfine structure due to the coupling with Nb nucleus proved their direct attachment to surface niobium sites (vide infra). Fig. 3B shows temperature dependence of the intensity of the IR signal of the superoxo species adsorbed on the surface of amorphous Nb_2O_5. The maximum intensity of this band was observed at 373 K. The $O_2^{-\bullet}$ species were not stable at 423 K, so they may act as reactive intermediates only for the reactions performed below this temperature.

The formation of peroxo species upon interaction of Nb_2O_5 with hydrogen peroxide was documented by the diagnostic infrared (Fig. 4) and Raman spectra (Fig. 5). The IR band at 888 cm^{-1} and the Raman band at 880 cm^{-1} arise from the O–O vibration of the surface peroxo species (O_2^{2-}) [16–19]. As expected, the intensity of the IR band increased with increasing contact time of the H_2O_2/H_2O solution with the surface of amorphous Nb_2O_5.

3.3. The function of pH

The pH value of the solution determines the transformation of peroxo into superoxo species (and vice versa) on the catalyst surface [10] by controlling the equilibria between solid (acidic hydroxyls) and liquid phase (H_2O_2/H_2O) components of the system. The interaction of acidic hydroxyls present on the surface of the investigated oxides with hydrogen peroxide can be described by the following equation:

$$H_2O_2 + \text{S-OH} = HO_2^- + \text{S-OH}_2^+ \quad (6)$$

where S denotes a surface site. Since pH of the isoelectric point (IEP) of amorphous Nb_2O_5 is 2.9, also the ionized surface sites S—O^- may

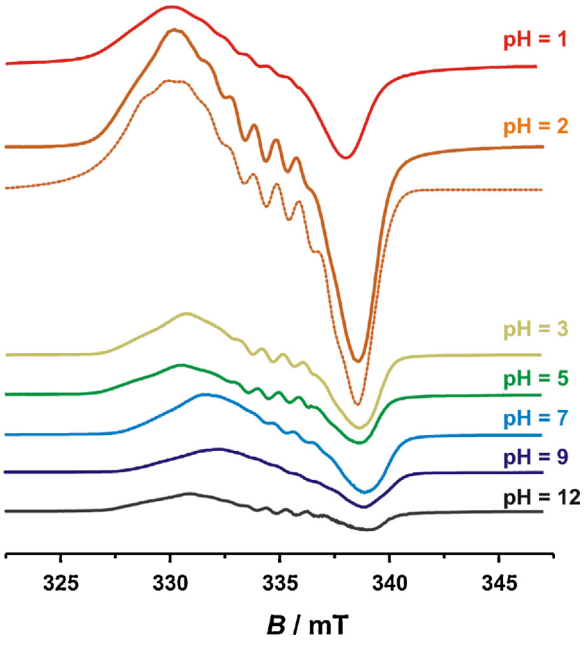

Fig. 6. Powder EPR spectra (77 K) of amorphous Nb_2O_5 treated with H_2O_2 at various pH. Dotted line (pH = 2) represents simulated spectrum.

participate in this reaction, shifting the equilibrium toward HO_2^- at pH > 3

Raman shift of Nb_2O_5 treated with H_2O_2 at different pH of the H_2O_2/H_2O solution presented in Fig. 5 shows development of a Raman band at 880 cm^{-1} assigned to the O—O vibration of peroxo species. A sudden increase of its intensity between pH = 2 and 3 correlates with IEP of the amorphous Nb_2O_5. Subsequent increase of pH to 5, 7 and 9 causes again an increase in the 880 cm^{-1} band intensity. That allows us to propose the following reactions for the basic media:

$$H_2O_2 + OH^- = HO_2^- + H_2O \quad (7)$$

$$HO_2^- + OH^- + S{-}Nb(V) = S{-}Nb(V){-}O_2^{2-} + H_2O \quad (8)$$

Contrary to the diamagnetic S—Nb(V)—O_2^{2-} peroxo surface species, the radical superoxo species O_2^-, detected earlier by IR, can be definitely proved by EPR. The EPR spectra of O_2^-shown in Fig. 6 exhibit a rhombic signal with a clearly resolved hyperfine structure due to ^{93}Nb (I = 9/2, 100%,). The spin-Hamiltonian parameters of this signal obtained by computer simulation are $g_{xx} = 2.000, g_{yy} = 2.020, g_{zz} = 2.032$, $|A_{yy}| = 1$ mT, with A_{xx} and A_{zz} remaining unresolved. The obtained parameters are intermediate between the parameters characteristic of electrostatically [20] and covalently [21] bound O_2^-species. Yet, they clearly indicate formation of the surface superoxo S-Nb(V) —$O_2^{-\bullet}$ adducts. The presence of the well resolved hyperfine coupling (A_{yy}) proves direct attachment of $O_2^-$to surface Nb(V) site. The intensity of the EPR signal strongly depends on the pH of H_2O_2/H_2O solution. The highest concentration of the $O_2^{-\bullet}$ radicals was obtained for pH around 2 (i.e. in the vicinity of the measured IEP of Nb_2O_5 equal to 2.9). Further increase in the pH value led to a substantial fall of the EPR signal.

Fig. 7 compares the intensity of the superoxo and peroxo surface species depending on pH. It is clear that with increasing pH the amount of peroxo species increases while the amount of superoxo radicals decreases. Both curves intersect in the vicinity of the isoelectric point of Nb_2O_5. Such strong dependence on pH suggests involvement of a proton transfer steps in the formation of the reactive oxygen species (see below).

The observed reactions of H_2O_2 with amorphous Nb_2O_5 imply not only that the kind of reactive oxygen species formed on the

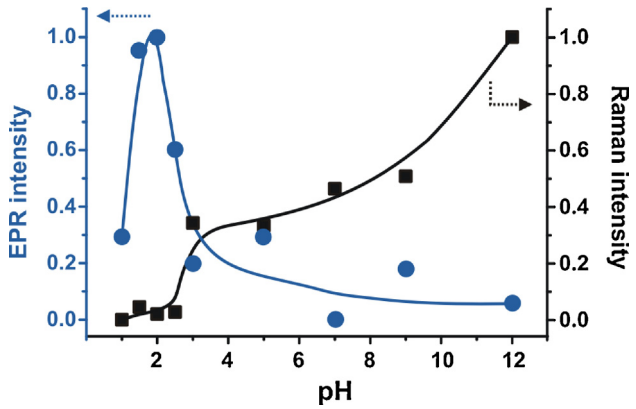

Fig. 7. Formation of O_2^-(EPR) and O_2^{2-}(Raman) species resulting from the interaction between Nb_2O_5 and H_2O_2 as a function of pH of the solution.

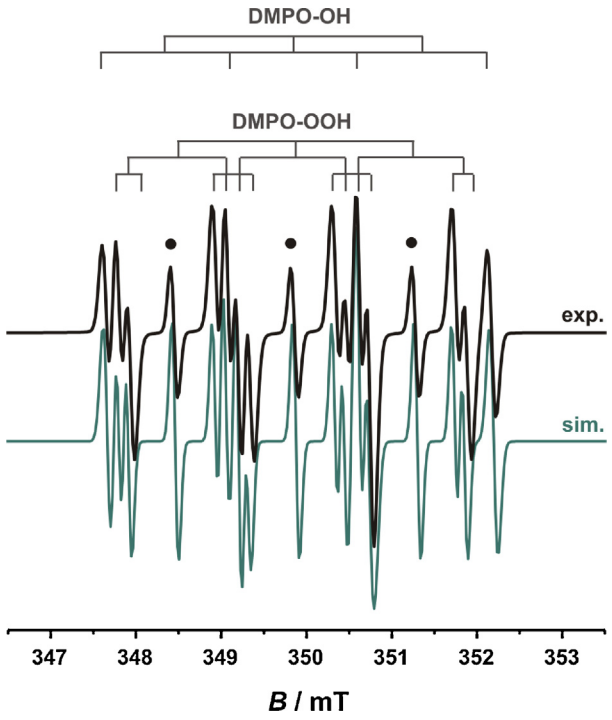

Fig. 8. Liquid phase experimental and simulated EPR spectra after the reaction of H_2O_2 with Nb_2O_5 in presence of DMPO spin trap. Dots indicate features of degradation products of the spin trap in reaction conditions.

surface is influenced by pH of the solution but also a double role of the niobium(V) oxide. In the initial steps of the reaction, Nb_2O_5 surface hydroxyls interact with H_2O_2 giving HO_2^- (Eq. 6). The second role of Nb_2O_5 is trapping of superoxo $O_2^{-\bullet}$ (and peroxo O_2^{2-}) species on the surface, leading to an increased production of the hydroxyl radicals (•OH). They are generated via electroprotic liquid phase reaction:

$$H_2O_{2(aq)} + HO_2^-{}_{(aq)} = {}^{\bullet}OH_{(aq)} + O_2^{-\bullet}{}_{(aq)} + H_2O_{(aq)} \quad (9)$$

followed by trapping of superoxo species

$$O_2^{-\bullet}{}_{(aq)} + S{-}Nb(V)_{(s)} = S{-}Nb(V){-}O_2^{-\bullet}{}_{(s)} \quad (10)$$

that substantially shifts the equilibrium (9) to the right. Hydroxyl and superoxo radicals generated in the liquid phase were simultaneously detected in an EPR experiment with the aid of a DMPO spin trap. The resulting isotropic EPR spectrum with its simulation is shown in Fig. 8. Two spin adducts contribute to this spectrum: DMPO-OOH (a_N = 1.41 mT, a_{H1} = 1.13 mT, and a_{H2} = 0.10 mT) and

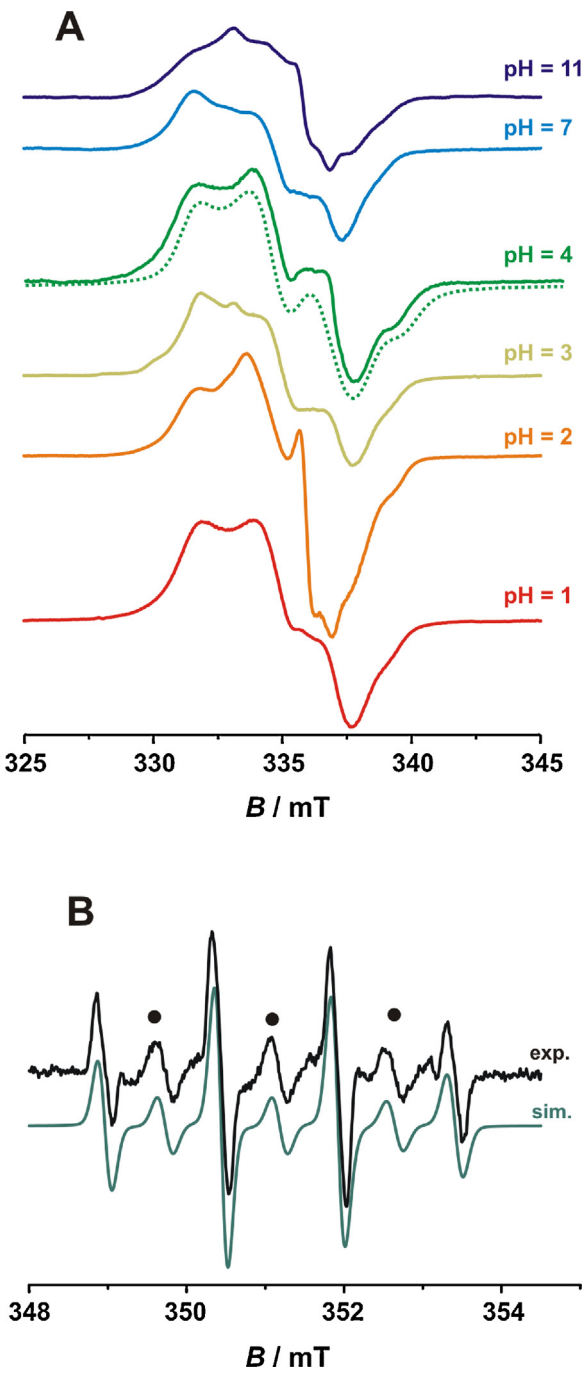

Fig. 9. (A) Powder EPR spectra of amorphous Ta_2O_5 treated with H_2O_2 at various pH (dotted line for pH = 4 represents simulated spectrum) and (B) corresponding liquid phase spectrum at pH around 4 in the presence of DMPO spin trap. Dots indicate features of degradation products of the spin trap in reaction conditions.

DMPO-OH (a_N = 1.55 mT, a_H = 1.43 mT), which result from the interaction between the spin trap and the $O_2^{-\bullet}$ and $^\bullet$OH radicals, respectively [22].

Similar conclusions were drawn from EPR measurements for the amorphous Ta_2O_5 treated with hydrogen peroxide (Fig. 9). Two types of surface $O_2^{-\bullet}$ radicals contribute to the observed powder EPR spectrum (g_{xx} = 2.000, g_{yy} = 2.021, g_{zz} = 2.037 and g_{xx} = 2.000, g_{yy} = 2.019, g_{zz} = 2.049). The obtained parameters are quite similar to those of niobia supported superoxo species. The intensity of the EPR signal also depends on pH (Fig. 9A), and is the highest at pH between 2 and 3 (again close to IEP of the amorphous Ta_2O_5). The overall signal intensity, as obtained by its double integration, indicates that the signal for tantalia supported superoxo species accounts for only 7% of the maximal intensity of niobia system. This points out that amorphous Ta_2O_5 is a worse scavenger for the superoxide species as compared with Nb_2O_5. Spin trapping revealed formation of $^\bullet$OH radicals (Fig. 9B) in the liquid phase (a_N = 1.49 mT, a_H = 1.46 mT). In contrast to Nb_2O_5, the signal due to DMPO-OOH spin adduct was missing, but the superoxo radicals were detected anyway at the catalyst surface (Fig. 9A).

Table 1
Results of cyclohexene oxidation with H_2O_2 (313 K, 40 h; acetonitrile (10 mL); cyclohexene (5 mmol); 30% hydrogen peroxide (5 mmol); catalyst: 0.1 g activated at 473 K).

Catalyst	Conversion and selectivity, %				
	Cyclohexene	H_2O_2	Epoxide	Diol	Other
After 24 h					
Nb_2O_5	48	–	0.2	30	69.8
Ta_2O_5	40	–	0.5	28	71.5
After 48 h					
Nb_2O_5	58	88	1	41	58
Ta_2O_5	38	89	3	38	59

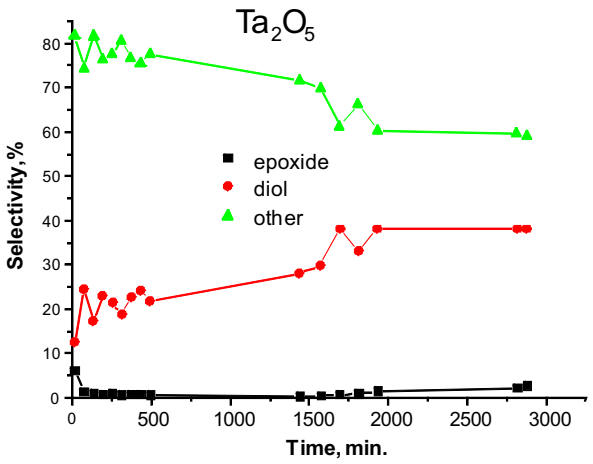

Fig. 10. Dependence of selectivity in cyclohexene oxidation on time of the reaction carried out on Ta_2O_5 (cyclohexene (5 mmol); 30% hydrogen peroxide (5 mmol); catalyst: 0.1 g activated at 473 K).

3.4. Catalytic activity

3.4.1. Cyclohexene oxidation

There are two main reaction pathways in the oxidation of cyclohexene [3,23] leading to different products. Electrophilic oxidation leads to epoxidation [24]. This route, directing the reaction towards epoxide, requires involvement of superoxo species. Next diols can be formed from the epoxide, when acidic centres present on the oxide surface causes opening of the epoxy ring. Epoxide and other products like cyclohexenyl hydroperoxide can be formed by the interaction of hydroxyl radicals with cyclohexane, as shown elsewhere [3]. Cyclohexene radical is formed in the first step of hydroxyl radical interaction. Since the isoelectric point of both niobium and tantalum oxides are below pH of the reaction medium (pH = 7), the surface becomes negative. This may significantly influence activity and selectivity of the catalyst.

Table 1 presents cyclohexene conversion and products selectivity analyzed after 24 and 48 h. The activity of the catalysts shown in this table expressed as cyclohexene conversion was different for both investigated oxides. The cyclohexene conversion was higher for Nb_2O_5, while product distribution was rather similar on both oxides. Selectivity to epoxide was negligible, hexanediol

Table 2
Catalytic activity in glycerol oxidation reaction, 333 K for 5 h (part of the data from ref. [5]).

Catalyst	Conditions of the reaction	Glycerol conv., %	Colour of catalyst after reaction	Selectivity to acids, %		
				Glyceric acid	Glycolic acid	Oxalic acid
Nb_2O_5 pH = 5	H_2O_2 (0.2 M)	10	Yellow	–	100	Traces
Nb_2O_5 pH = 5	H_2O_2 (0.6 M)	14	Yellow	10	90	Traces
Nb_2O_5 pH = 9.5	H_2O_2 (0.6 M)/ NaOH	18	White	5	95	Traces
Nb_2O_5 pH = 2.5	H_2O_2 (0.6 M)/ HNO_3	Almost inactive	Yellow	Traces	Traces	–
Ta_2O_5 pH = 5	H_2O_2 (0.6 M)	Almost inactive	White	Traces	Traces	–

was produced in significant amounts, but the highest selectivity was observed to different hydroxylated cyclohexanes. For both catalysts the selectivity to hexanediol was lower after 24 h than after 48 h of the reaction. As an example, the reaction profile for Ta_2O_5 is shown in Fig. 10. It is clear that hydroxylated products are intermediates in production of hexanediol, which is not formed from the epoxide precursor. On the basis of these results one can postulate that superoxo species are spectators and do not participate directly in the oxidation of cyclohexene since the epoxide occurred in minor amounts only. In fact the surface concentration of superoxo species at pH = 7 is very low (Fig. 7). The hydroxyl radicals produced by electroprotic liquid phase reaction ($H_2O_2 + HO_2^- = {}^\bullet OH + O_2^{-\bullet} + H_2O$) are the active species in the formation of hydroxylated cyclohexene and finally cyclohexenediol. The role of amorphous oxide is to trap the concurrently produced superoxide radicals ($O_2^{-\bullet}$ + S—Nb(V) = S—Nb(V)—$O_2^{-\bullet}$), shifting the reaction equilibrium toward $^\bullet$OH radical formation.

3.5. Glycerol oxidation

Oxidation of glycerol with hydrogen peroxide was described phenomenologically in our previous paper in detail [5]. In this article we consider the role of the reactive oxygen species in this process. For this purpose relevant data from previous paper are shown in Table 2, and they are completed by the new results obtained at different pH of the reaction medium. There is a significant difference in the activity of Nb_2O_5 and Ta_2O_5 in glycerol oxidation, the latter being almost inactive. According to the mechanism of glycerol oxidation [25,26], glycolic acid is formed from glyceraldehyde (or dihydroxyacetone) via formation of hydroxypuruvic aldehyde and hydroxypuruvic acid as the intermediates. The hydroxyl radicals formed from H_2O_2 take part in the dehydrogenation of glycerol towards glycerolate (via H-abstraction from one of the primary hydroxyl groups), the latter being an intermediate in formation of final products. Selectivity to glycolic acid is controlled by the presence of H_2O_2, which is responsible for oxidative C—C bond cleaving.

Glycerol conversion on Nb_2O_5 depended on the amount of the added hydrogen peroxide and a basic (NaOH) or an acidic (HNO_3) reaction medium (Table 2). The characteristic yellow colour of the sample that resulted from the formation of surface peroxo species did not change after the reaction, suggesting that another species was responsible for the activity in this process. Interestingly, when NaOH was added to the reaction medium, the glycerol conversion was higher, and the catalyst becomes white after the reaction. At pH 9.5 Nb_2O_5 revealed the highest activity and selectivity to glycolic acid (Table 2). Under these conditions superoxo species transform to yellow peroxo species. The latter are definitely less active in glycerol oxidation than the hydroxyl radicals produced by the interaction of the excess of H_2O_2 with hydrosuperoxo groups. Niobia surface again allows for stabilization of the spectator superoxo species and by shifting the reaction equilibrium in Equation (9), increases the amount of the hydroxyl radicals, which act as the key active species for this reaction. The increase in OH^- by NaOH admission also leads to shift of the $O_2^{-\bullet} + {}^\bullet OH = OH^- + O_2$ equilibrium to the left, enhancing thereby production of the hydroxyl radicals. As a result reaction rate is enhanced. It is important to add that at pH = 2.5, i.e. close to its IEP value, niobia was almost inactive. It supports the importance of not only aqueous hydroxyls but also surface in catalytic glycerol oxidation.

4. Conclusions

The UV–Vis, Raman, and EPR (including spin trapping by DMPO) investigations revealed high ability of the amorphous Nb_2O_5 to form superoxo, peroxo, and hydroxyl reactive oxygen species (ROS) upon contact with hydrogen peroxide. The ability of ROS generation on Ta_2O_5 in analogous conditions was distinctly lower. The ROS nature and abundance can effectively be controlled by pH variation of the reaction medium in relation to the isoelectric point of the catalyst. An electroprotic mechanism of ROS formation was proposed, where the $H_2O_2 + HO_2^- = {}^\bullet OH + O_2^{-\bullet} + H_2O$ equilibrium plays a central role. Amorphous state of the Nb_2O_5 and Ta_2O_5 is beneficial since they act as a sponge for trapping $O_2^{-\bullet}$ and O_2^{2-}, shifting the electroprotic equilibrium toward $^\bullet$OH radicals. Among the reactive oxygen species formed upon the complex interaction of H_2O_2 with niobia and tantalia surface, hydroxyl radicals are the most active in catalytic oxidation of glycerol and cyclohexene.

Acknowledgements

National Science Centre in Poland (Grant No. 2011/01/B/ST5/00847) is acknowledged for the financial support of this work. Acknowledgement is made also to CBMM Company (Brazil) for supplying niobium(V) oxide. The EPR and Raman measurements were carried out with the equipment purchased thanks to the financial support of the European Regional Development Fund in the framework of the Polish Innovation Economy Operational Program (contract no. POIG.02.01.00-12-023/08). Authors thank Dr. K. Góra-Marek (Jagiellonian University, Krakow) for help in IR in situ measurements and Ms Marta Falkowska (Adam Mickiewcz University, Poznan) for technical assistance in UV-Vis measurements.

References

[1] R.A. Sheldon, I.W.C.E. Arends, H.E.B. Lempers, Catal. Today 41 (1998) 387–407.
[2] M. Ziolek, Catal. Today 90 (2004) 145–150.
[3] E. Jorda, A. Tuel, R. Teissier, J. Kervennal, J. Catal 175 (1998) 93–107.
[4] J. Haber, in: G. Ertl, H. Knozinger, J. Weitkamp (Eds.), Handbook of Heterogeneous Catalysis, vol. 2, VCH Verlagsgesellschalf mbH, Wienheim, 1997, p. p2253.
[5] M. Ziolek, I. Sobczak, P. Decyk, L. Wolski, Catal. Commun. 37 (2013) 85–91.
[6] T. Spalek, P. Pietrzyk, Z. Sojka, J. Chem. Inf. Model 45 (2005) 18–29.
[7] K. Sadowska, A. Wach, Z. Olejniczak, P. Kuśtrowski, J. Datka, Micropor. Mesopor. Mater. 167 (2013) 82–88.
[8] L.G. Hubert-Pfalzgraf, in: R. Bruce King (Ed.), Encyclopedia of Inorganic Chemistry, 5, Wiley, John & Sons, 1994, pp. 2444–2462.
[9] L. Moreno-Real, E.R. Losilla, M.A.G. Aranda, M. Martinez-Lara, S. Bruque, M. Gabas, J. Solid State Chem. 137 (1998) 289–294.
[10] D. Srinivas, P. Manikandan, S.C. Laha, R. Kumar, P. Ratnasamy, J. Catal. 217 (2003) 160–171.
[11] S. Khabtou, T. Chevreau, J.C. Lavalley, Microporous Mater. 3 (1994) 133–148.
[12] S. Chenevarin, F. Thibault-Starzyk, Angew. Chem. Int. Ed. 43 (2004) 1155–1158.
[13] M. Ziolek, I. Nowak, J.C. Lavalley, Catal. Lett. 45 (1997) 259–265.
[14] M. Che, T.J. Tench, Adv. Catal. 32 (1983) 1–148.
[15] M. Anpo, M. Che, B. Fubini, E. Garone, E. Giamello, M.C. Paganini, Top. Catal. 8 (1999) 189–198.
[16] J. Sala-Pala, J. Roue, J.E. Guerchais, J. Mol. Catal. 7 (1980) 141–148.
[17] D. Bayot, M. Devillers, Coordin. Chem. Rev. 250 (2006) 2610–2626.
[18] F.P. Cardoso, A.E. Nogueira, P.S.O. Patrício, L.C.A. Oliveira, J. Brazil. Chem. Soc. 23 (2012) 702–709.
[19] E.I.Ch. Wachs, A. Roberts, Chem. Soc. Rev. 39 (2010) 5002–5017.
[20] M. Chiesa, E. Giamello, M.C. Paganini, Z. Sojka, D.M. Murphy, J. Chem. Phys. 116 (2002) 4266–4274.
[21] P. Pietrzyk, K. Podolska, T. Mazur, Z. Sojka, J. Am. Chem. Soc. 133 (2011) 19931–19943.
[22] G.R. Buettner, Free Radical Biol. Med. 3 (1987) 259–303.
[23] O.A. Kholdeeva, T.A. Trubitsina, M.N. Timofeeva, G.M. Maksimov, R.I. Maksimovskaya, V.A. Rogov, J. Mol. Catal. A: Chem. 232 (2005) 173–178.
[24] M.E. Jung, G. Piizzi, Org. Lett. 5 (2003) 137–140.
[25] W.C. Ketchie, M. Murayama, R.J. Davis, Topics Catal. 44 (2007) 307–317.
[26] F. Porta, L. Prati, J. Catal. 224 (2004) 397–403.